Journal of Glaciology, Vol. 46, *No.* 154, 2000

A flow model for the polar caps of Mars

J. F. Nye
H. H. Wills Physics Laboratory, University of Bristol, Tyndall Avenue, Bristol BS8 1TL, England

ABSTRACT. A mechanical model with circular symmetry is examined to test the hypothesis that the Martian ice caps are composed of flowing water ice, together with some rock debris. In contrast with most or all previous models, no assumption of a steady state is made. Instead the accumulation and ablation is assumed to be insignificant, and it is suggested that after a sufficient time the profile would have settled down to a particular collapsing form calculated by Halfar (1983). Higher modes of flow would have decayed relatively quickly. To calculate the time constant, it is necessary to consider carefully the distribution of temperature with depth. The time constant is sensitive to the grain-size, which is assumed to be 1–10 mm and is a significant unknown, as is also the effect of preferred crystal orientation. Apart from this, the main uncertainty is the value of the upward heat flux. With a heat flux of 30 mW m^{-2}, the water-ice hypothesis is consistent with an age of about 10^7 years for both the north and the south polar caps, the north cap being the younger by a factor of about 7.

1. INTRODUCTION

The permanent polar caps on Mars are recognizable from the topography as domes rising above the surrounding layered terrain (Zuber and others, 1998; Smith and others, 1999; Schenk and Moore, in press; see also the extensive review by Clifford and others, 2000). One has to distinguish them from the seasonal caps, whose visible extent varies through the Martian year and which are probably surface layers of solid carbon dioxide. There are such seasonal carbon dioxide surface layers in both the north (Haberle and Jakosky, 1990; Kieffer, 1990) and the south (Herkenhoff and Murray, 1990; Paige and others, 1990). On the other hand, it is plausible to suppose that the north and south permanent polar caps of Mars are made of water ice, possibly with a substantial admixture of rock particles, but this is not yet firmly established. Water ice is observed in the north (Kieffer, 1990), but an alternative hypothesis that the entire thickness of the south polar cap is solid carbon dioxide seems to fail on mechanical grounds; Nye and others (2000) concluded that such a material is far too weak to support a cap of the observed height of 3000 m for the necessary time of 10^7 years.

The flow model used in Nye and others (2000) was comparatively crude in its treatment of the effect of temperature on the flow, but the simplification was justified because the solid-carbon-dioxide hypothesis gave lifetimes that were orders of magnitude too small even on the most extreme assumptions. However, to use such a flow model to make a fuller test of the assumption that both caps are made of water ice requires a more careful treatment of the effect of temperature, and that is the purpose of the present paper.

Budd and others (1986) took full account of the complex topography of the north cap by a numerical approach, and related their results to a steady state. In contrast, the present paper uses analytical methods to study an ice cap having circular symmetry and does not assume a steady state. It calculates what flow would occur in a cap of carefully chosen profile in the absence of any accumulation or ablation (it being supposed that there has been none of significance in the relevant period). The central parts will tend to fall, the outer parts will rise, and at the same time the perimeter will move outwards.

A crucial question is what profile to assume, because slight differences in the profile result in totally different distributions of the rate of change of thickness. The profile chosen will, in fact, be close to, but not identical with, that of the Vialov (1958) model, as seen in Figure 1. The rather similar Nye (1959) model is less appropriate for comparison here because it is based on a sliding law rather than on a flow law. Both the Vialov and the Nye model assumed a steady state and a uniform distribution of accumulation; there was accumulation over the cap but no ablation. The rate of discharge of ice across the outer edge was therefore finite although the thickness was zero; as a result, the velocity at the edge was infinite. For a terrestrial ice cap that is bounded by the sea, perhaps this singularity in the model could be tolerated; it corresponds to concentrating all the ablation into the perimeter and not allowing the cap to expand sideways. For an ice cap that ends on land and spreads laterally under its weight, it is not appropriate.

The present model is quite different in conception, in that it calculates for zero accumulation and ablation and derives an evolving profile (a changing shape) from a similarity hypothesis. Most notably, it avoids the edge singularity in the above models and allows the cap to spread laterally.

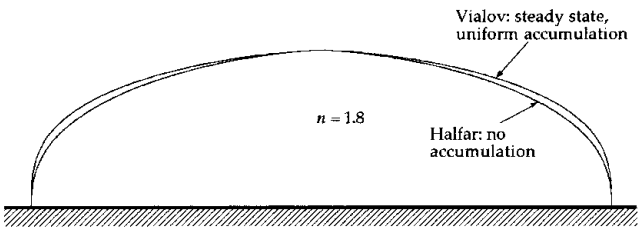

Fig. 1. Comparison of two profiles, the Vialov (1958) model and the present model, both with $n = 1.8$.

https://doi.org/10.3189/172756500781833151 Published online by Cambridge University Press

2. THE MODEL

The required solution of the flow equations, a similarity solution, was introduced into glaciology by Halfar (1981) for two-dimensional flow and Halfar (1983) for radial flow, as here. Hindmarsh (1990) has discussed the two-dimensional solution. Here, prompted by the latter paper, we deduce the radial-flow solution from a similarity hypothesis, rather than simply state it. Our model is then essentially the same as that of Halfar (1983), but with two additions. First, it is found possible to include isostatic depression of the base with minimal change in the mathematics; second, we take account of the effect on the flow law of the variation of temperature with depth and with time.

At radius r and time t the thickness is $h(r,t)$ (Fig. 2a). The thickness at the centre $h(0,t)$ is denoted by $h_0(t)$, and the radius of the base is $r_0(t)$. The base, originally horizontal, is depressed by the weight of the ice by a fraction f of the ice thickness, that is by $fh(r,t)$, so that the elevation of the upper surface is $(1-f)h(r,t)$. Define a scaled radial co-ordinate $\rho = r/r_0(t)$ and a scaled thickness η (Fig. 2b)

$$\eta = \frac{h(r,t)}{h_0(t)} = \frac{h(r_0\rho,t)}{h_0(t)} = \eta(\rho,t)\,. \tag{1}$$

We look for a solution of the flow equations in which $\eta = \eta(\rho)$, independent of t; that is, the scaled shape keeps the same analytical form. It does *not* remain geometrically similar (Fig. 3); the aspect ratio changes.

Let $q(r,t)$ be the radial flux (volume per unit time crossing an area of height h and unit circumferential length). By conservation of volume

$$\left(\frac{\partial(qr)}{\partial r}\right)_t + r\left(\frac{\partial h}{\partial t}\right)_r = 0\,, \tag{2}$$

the second term of which is

$$r\left(\frac{\partial h}{\partial t}\right)_r = r_0\rho\left(\frac{\partial(h_0\eta)}{\partial t}\right)_r = r_0\rho\left[\dot{h}_0\eta + h_0\frac{\mathrm{d}\eta}{\mathrm{d}\rho}\left(\frac{\partial\rho}{\partial t}\right)_r\right]. \tag{3}$$

Because the overall volume is fixed and $\eta = \eta(\rho)$, $(\mathrm{d}/\mathrm{d}t)(h_0 r_0^2) = 0$, and hence $\dot{r}_0 = -(r_0/2h_0)\dot{h}_0$. Since $\rho = r/r_0$,

$$\left(\frac{\partial\rho}{\partial t}\right)_r = -\frac{r}{r_0^2}\dot{r}_0 = \frac{\rho}{2h_0}\dot{h}_0\,. \tag{4}$$

Thus, from Equation (3)

$$r\left(\frac{\partial h}{\partial t}\right)_r = r_0\rho\dot{h}_0\left(\eta + \frac{1}{2}\rho\frac{\mathrm{d}\eta}{\mathrm{d}\rho}\right) = \frac{1}{2}r_0\dot{h}_0\frac{\mathrm{d}}{\mathrm{d}\rho}(\rho^2\eta)\,, \tag{5}$$

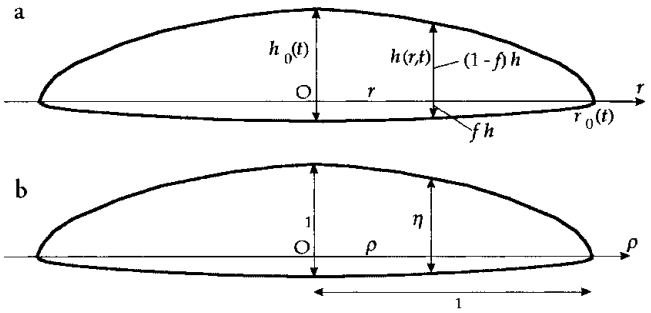

Fig. 2. Notation for the model cap: (a) dimensional lengths, (b) scaled dimensionless lengths.

and Equation (2) becomes, in terms of ρ

$$\left(\frac{\partial(q\rho)}{\partial\rho}\right)_t + \frac{1}{2}r_0\dot{h}_0\frac{\mathrm{d}}{\mathrm{d}\rho}(\rho^2\eta) = 0\,. \tag{6}$$

The crucial step is in Equation (5), where $(\partial/\partial t)_r$ is converted to $\mathrm{d}/\mathrm{d}\rho$. Equation (6) may now be integrated with respect to ρ at constant t; thus

$$q\rho + \frac{1}{2}r_0\dot{h}_0\,.\,\rho^2\eta = g(t),\ \text{say}\,. \tag{7}$$

Dividing by ρ, and demanding that $q = 0$ at $\rho = 0$ for all t, sets $g(t) \equiv 0$, so that

$$q = -\frac{1}{2}r_0\dot{h}_0\,.\,\rho\eta\,. \tag{8}$$

We now introduce a flow law of the form

$$\dot{\varepsilon}_1 = A_\mathrm{D}\exp(-Q/R_\mathrm{G}T)\sigma^n\,,$$

where $\dot{\varepsilon}_1$ is the uniaxial compression rate of polycrystalline ice under uniaxial compressive stress σ, A_D and n are constants, Q is the activation energy, R_G is the gas constant ($8.3143\,\mathrm{J\,K^{-1}mol^{-1}}$) and T is the absolute temperature. The corresponding relation for the simple shear rate $\dot{\gamma}$ under shear stress τ is

$$\dot{\gamma} = E\exp(-Q/R_\mathrm{G}T)\tau^n\,, \quad E = 3^{\frac{1}{2}(n+1)}A_\mathrm{D}\,. \tag{9}$$

It is convenient to assume at first that the temperature is uniform in space and constant with time, but later this restriction will be removed. Taking the flow of the cap to be predominantly by horizontal shearing and assuming the slope α of the top surface to be small, we have at given radius and time (Nye, 1952)

$$q = Ch^{n+2}\alpha^n \tag{10}$$

$$= Ch^{n+2}[-(1-f)(\partial h/\partial r)_t]^n\,,$$

$$= C\frac{h_0^{2n+2}}{r_0^n}\,.\,\eta^{n+2}[-(1-f)\,\mathrm{d}\eta/\mathrm{d}\rho]^n\,, \tag{11}$$

where

$$C = E\exp(-Q/R_\mathrm{G}T)(\rho' g)^n/(n+2)\,. \tag{12}$$

ρ' is the density, and the full stop in Equation (11) separates the time-dependent part from the ρ-dependent part. $\partial h/\partial r$ and $\mathrm{d}\eta/\mathrm{d}\rho$ are negative. Note that the flow law of ice at the appropriate temperature is included in the constant C. At the extreme edge the slope becomes infinite, and Relation (10) must break down; it should be replaced by different physics, but because the region affected is very narrow we shall ignore this defect. A similar problem arises in all

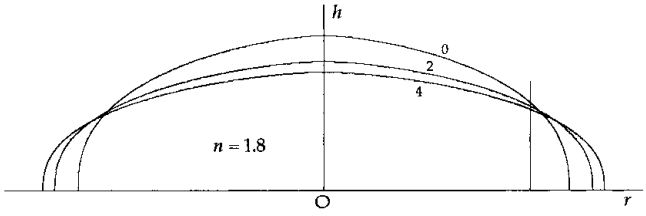

Fig. 3. The thickness distribution for $n = 1.8$ at three successive instants $t = 0,\ 2t_0,\ 4t_0$. The intersection point of successive curves moves outwards as the profile collapses, because $\partial h/\partial t = 0$ at fixed ρ not fixed r. The value of r for which $\partial h/\partial t = 0$ at $t = 0$ is indicated.

https://doi.org/10.3189/172756500781833151 Published online by Cambridge University Press

models of this kind. In view of Equation (8) the equation to be integrated is therefore

$$C(1-f)^n \frac{h_0^{2n+2}}{r_0^n} . \eta^{n+2}(-\mathrm{d}\eta/\mathrm{d}\rho)^n = -\frac{1}{2} r_0 \dot{h}_0 . \rho\eta . \quad (13)$$

After division by η, the variables may now be separated to give

$$2C(1-f)^n \eta^{n+1}(-\mathrm{d}\eta/\mathrm{d}\rho)^n = K\rho \quad (14)$$

and

$$\dot{h}_0 = -K(h_0^{2n+2}/r_0^{n+1}) , \quad (15)$$

where K is a constant.

The thickness distribution will follow from integrating Equation (14):

$$-\int_1^\eta \eta^{1+1/n}\,\mathrm{d}\eta = \frac{1}{1-f}\left(\frac{K}{2C}\right)^{1/n} \int_0^\rho \rho^{1/n}\,\mathrm{d}\rho .$$

First, use for the upper limits $\eta = 0$ at $\rho = 1$, to yield the value of K as

$$K = 2C(1-f)^n \left(\frac{n+1}{2n+1}\right)^n . \quad (16)$$

Then, on integration, the scaled thickness distribution is

$$\rho^{1+1/n} + \eta^{2+1/n} = 1 , \quad (17)$$

as found by Halfar (1983) for the case $f = 0$. It is fortunate that non-zero f makes no difference to this equation.

Integration of Equation (15) gives the time dependence. It is convenient to think of $t = 0$ as the present, when the central height is $H_0 = h_0(0)$ and the radius of the cap is R_0 say. Then $h_0 r_0^2 = \text{const.} = H_0 R_0^2$, and Equation (15) becomes

$$\dot{h}_0 = -K(H_0 R_0^2)^{-(n+1)/2} h_0^{(5/2)(n+1)} .$$

This integrates to give the decay of the central height as

$$h_0(t) = H_0\left(1 + \frac{t}{t_0}\right)^{-2/(5n+3)} \quad (18)$$

with, using Equation (16),

$$t_0 = \frac{1}{C(1-f)^n(5n+3)} \left(\frac{2n+1}{n+1}\right)^n \frac{R_0^{n+1}}{H_0^{2n+1}} . \quad (19)$$

$t = -t_0$ is the time at which the central height is asymptotically infinite (Fig. 4). Equation (19) will be central in what follows.

Since $h_0 r_0^2$ is constant the corresponding equation for the expansion of the outer rim is

$$r_0(t) = R_0\left(1 + \frac{t}{t_0}\right)^{1/(5n+3)} , \quad (20)$$

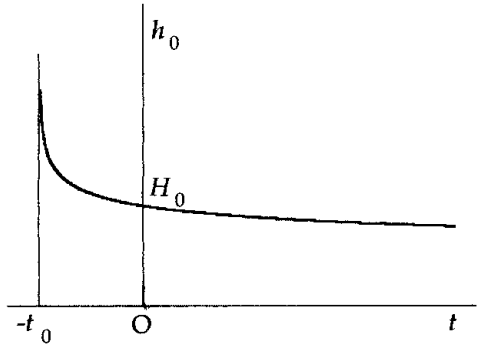

Fig. 4. The decay of the central thickness with time.

and the aspect ratio diminishes according to

$$\frac{h_0(t)}{r_0(t)} = \frac{H_0}{R_0}\left(1 + \frac{t}{t_0}\right)^{-3/(5n+3)} . \quad (21)$$

In Equation (19) R_0 and H_0 are observable quantities, C can be estimated as discussed below, and so, with an estimation of the isostatic fraction f, t_0 can be calculated. In the model the cap spreads out from an initial delta-function shape at $t = -t_0$. In Figure 3, $h(r)$ is computed at successive times $t = 0$ (the present) and $2t_0$, $4t_0$ (in the future) by using Equations (17), (18) and (20). Halfar (1983) has shown that the resulting evolving profile is stable against all perturbations that preserve the total volume. That is the justification for using this special profile, and its decay with time, as a model of the real situation. Whatever the real history of the cap may have been, the profile would have settled down quite quickly (in a time much less than t_0) to the steady mode calculated; an analogous situation occurs when syrup falls from a spoon on to a plate to form a spreading dome. t_0 is the age of the model cap. Making the assumption that the real caps have evolved to their present shapes by non-Newtonian viscous spreading, we shall interpret t_0 as the age of the real cap, even though it began in a different way from the model cap.

3. ESTIMATION OF C

By taking C, which incorporates the flow law, as a constant, the calculation has assumed that the temperature is both uniform in space and constant with time. We shall continue to assume that the surface temperature remains constant with time (in the absence of reliable evidence to the contrary), thus ignoring the obliquity cycle of 1.25×10^5 years (Clifford and others, 2000), but we wish to take explicit account of the fact that the temperature is non-uniform with depth by using a parallel-sided slab model. Specifically, with z measured downwards from the surface, we assume a non-uniform temperature gradient that conducts the geothermal heat flux ϕ upwards:

$$\phi = k(T)\frac{\partial T}{\partial z} . \quad (22)$$

The gradient is non-uniform because the thermal conductivity k depends upon temperature. (In terrestrial ice caps an additional non-uniformity is caused by advection due to the downward vertical motion of the ice, but in the present model the slowness of the downward motion makes such an effect negligible.) The flow law now depends on depth.

If u is the outward velocity at depth z we have, at radius r, where the surface slope is α,

$$-\frac{\mathrm{d}u}{\mathrm{d}z} = \dot{\gamma} = E\exp(-Q/R_\mathrm{G}T)\tau^n$$
$$= E\exp(-Q/R_\mathrm{G}T)(\rho' g\alpha)^n z^n .$$

Hence, assuming zero velocity on the bed,

$$u = \int_0^u \mathrm{d}u = E(\rho' g\alpha)^n \int_z^h \exp[-Q/R_\mathrm{G}T(z)]z^n\,\mathrm{d}z . \quad (23)$$

https://doi.org/10.3189/172756500781833151 Published online by Cambridge University Press

A further integration gives the discharge as

$$q = \int_0^h u\,\mathrm{d}z = E(\rho' g\alpha)^n \int_0^h \mathrm{d}z \int_z^h \mathrm{d}z \exp[-Q/R_\mathrm{G}T(z)]z^n\,. \tag{24}$$

It is useful to define an effective temperature T_eff as the uniform temperature that would give the same discharge as the actual non-uniform temperature. If $T(z)$ in the above integrand is replaced by a constant T_eff, the double integral becomes $\exp(-Q/R_\mathrm{G}T_\mathrm{eff})\,.\,h^{n+2}/(n+2)$, as used in Equation (12). Thus T_eff is given by

$$\int_0^h \mathrm{d}z \int_z^h \mathrm{d}z \exp[-Q/R_\mathrm{G}T(z)]z^n = \exp(-Q/R_\mathrm{G}T_\mathrm{eff})\,.\,h^{n+2}/(n+2)\,. \tag{25}$$

To apply Equation (19), where C is constant, it is necessary to choose a single value for T_eff that is representative of the whole cap and indeed of its whole history. This means a single representative value of h for the thermal calculation. Therefore, to choose h we first average η over the area of the ice cap — for $n = 1.8$ (see below) the average is 0.6766 — and hence, using the observed central elevation with an assumed f, we find the average thickness at $t = 0$ (the present). Then, to take some account of the greater thickness in the past, we scale it up by a factor corresponding to halfway through the period of interest, $t = -t_0$ to 0, found from Equation (18) as $2^{2/(5n+3)}$; for $n = 1.8$ this amounts to an increase of 12% (the decay curve in Figure 4 is quite flat).

Having chosen h in Equation (25), the next task is to evaluate the function $T(z)$ using Equation (22). The temperature dependence of the thermal conductivity of pure ice is well represented by the relation (Hobbs, 1974, p. 358)

$$k(T) = \frac{A}{T} + B, \quad A = 488.19\,\mathrm{W\,m^{-1}},$$
$$B = 0.4685\,\mathrm{W\,m^{-1}\,K^{-1}}\,.$$

By integration of Equation (22) downwards from the surface, where $T = T_\mathrm{s}$,

$$z(T) = \frac{1}{\phi}\left[A \ln\frac{T}{T_\mathrm{s}} + B(T - T_\mathrm{s})\right].$$

To invert this to find $T(z)$ we select a desired value z_0 and solve the equation $z_0 - z(T) = 0$ numerically for T, by Newton's method, given the gradient $z'(T) = k(T)/\phi$, from Equation (22). This gives $T(z)$ for a chosen value of ϕ. The double integral in Equation (25) is evaluated by Simpson's rule, and hence T_eff, is found.

The numerical consequences of applying these results, especially Equation (19), to the Martian caps will be discussed in section 5. The next section will trace some formal consequences of the model.

4. REMARKS ABOUT THE FLOW SOLUTION

4.1. Shapes of craters

A small circle (crater) drawn at an instant on the surface of the cap will, in general, become elliptical, according to the difference between the radial and the circumferential strain rates. However, we now show that in the Halfar model these strain rates are very nearly equal, so that a circular crater remains approximately circular.

Let $\bar{u}$ denote the outward radial velocity averaged through the thickness. Then from Equation (8)

$$\bar{u} = \frac{q}{h} = \frac{q}{h_0\eta} = -\frac{1}{2}\frac{r_0\dot{h}_0}{h_0}\rho\,. \tag{26}$$

Thus $\bar{u}$ varies linearly with ρ. The radial strain rate is

$$\dot{\varepsilon}_r = \left(\frac{\partial\bar{u}}{\partial r}\right)_t = \frac{1}{r_0}\left(\frac{\partial\bar{u}}{\partial\rho}\right)_t = -\frac{1}{2}\frac{\dot{h}_0}{h_0}\,, \tag{27}$$

and the circumferential strain rate is

$$\dot{\varepsilon}_\theta = \frac{\bar{u}}{r} = \frac{\bar{u}}{r_0\rho} = -\frac{1}{2}\frac{\dot{h}_0}{h_0}\,. \tag{28}$$

It is remarkable that not only are the two rates identical but they are independent of ρ: the strain rate, averaged through the thickness, is not only isotropic but uniform over the cap at any given time. It follows from constancy of volume that the vertical strain rate $\dot{\varepsilon}_z = \dot{h}_0/h_0$ will also be uniform. These results are a consequence simply of the scaling assumption that $\eta = \eta(\rho)$, independent of t, together with conservation of volume; they are independent of the assumed flow law.

To calculate the change of shape of a crater, we need to consider not $\bar{u}$ but the surface velocity u_s. From Equation (23) with (12), assuming uniform temperature, the relation between them is $u_\mathrm{s} = [(n+2)/(n+1)]\bar{u}$. Thus the radial strain rate at the surface is $\dot{\varepsilon}_{rs} = [(n+2)/(n+1)]\dot{\varepsilon}_r$. On the other hand, the circumferential strain rate at the surface is still $\dot{\varepsilon}_\theta$ as calculated above, so there is now a difference between them. Over the time interval $t = -T$ to 0 a small circle of radius $\bar{r}$ becomes an ellipse with semiaxes a (radial) and b (circumferential) given by

$$a = \bar{r}\exp\int_{-T}^0 \dot{\varepsilon}_{rs}\,\mathrm{d}t, \quad b = \bar{r}\exp\int_{-T}^0 \dot{\varepsilon}_\theta\,\mathrm{d}t\,;$$

so that

$$a/b = \exp\left[\left(\frac{n+2}{n+1} - 1\right)\int_{-T}^0 \dot{\varepsilon}_\theta\,\mathrm{d}t\right] = \exp\left(\frac{1}{n+1}\int_{-T}^0 \dot{\varepsilon}_\theta\,\mathrm{d}t\right).$$

Equation (28) with (18) gives $\dot{\varepsilon}_\theta = 1/[(5n+3)(t_0+t)]$, so that, carrying out the integration,

$$\frac{a}{b} = \left(\frac{t_0}{t_0 - T}\right)^{1/(n+1)(5n+3)}.$$

Taking, for example, $T = \frac{1}{2}t_0$, we find

$$\frac{a}{b} = 2^{1/(n+1)(5n+3)}\,.$$

For $n = 1.8$ the ratio is 1.0208. Using u_s instead of $\bar{u}$ has changed the result by merely 2%. The conclusion is that a crater that was initially circular would have remained nearly so. But would a crater tend to be circular when it was first formed? The answer is probably yes. Melosh (1989), writing on craters in general, says "it has long been known that the angle of impact has little effect on the shape of the ... crater, except for very low angles of incidence". Highly oblique incidence is quite rare, and systematically elliptical craters have not been reported on the Martian caps. Although this would support our theoretical conclusion that flow does not cause

https://doi.org/10.3189/172756500781833151 Published online by Cambridge University Press

appreciable distortion, it has to be added that in fact very few, if any, definite craters have been seen on the caps at all.

The uniformity of the radial (longitudinal) strain rate, averaged over depth, in this model is quite different from what is usually found in a valley glacier (Paterson, 1994). There the velocity is generally expected to reach a maximum in the neighbourhood of the equilibrium line, thus giving longitudinal extension in the upper parts and compression in the lower parts. However, this difference seems to be no reason for rejecting the Halfar model.

4.2. Accumulation and ablation

Figure 3 shows that the surface of the model cap falls in the central part and rises in an outer annulus. $(\partial h/\partial t)_r$ has to be distinguished from the derivative following the ice, $\mathrm{d}h/\mathrm{d}t$, which is equal to $h\dot{\varepsilon}_z$, $\dot{\varepsilon}_z$ being uniform. The relation between them is

$$\left(\frac{\partial h}{\partial t}\right)_r = \frac{\mathrm{d}h}{\mathrm{d}t} - \bar{u}\left(\frac{\partial h}{\partial r}\right)_t .$$

The two terms on the right have opposite signs, and so can cancel. The relation $\bar{u} = q/h$ and Equation (8) for q transform this to

$$\left(\frac{\partial h}{\partial t}\right)_r = \dot{h}_0\left[\eta + \frac{1}{2}\rho\left(\frac{\mathrm{d}\eta}{\mathrm{d}\rho}\right)\right].$$

Equation (18) for the time dependence of h_0, and Equation (17) for η, then give

$$\left(\frac{\partial h}{\partial t}\right)_r = \frac{\dot{H}_0}{t_0}\frac{1}{5n+3}\left(1+\frac{t}{t_0}\right)^{-5(n+1)/5n+3}$$
$$\cdot\,(1-\rho^{1+1/n})^{-(n+1)/(2n+1)}\left(\frac{5n+3}{2n+1}\rho^{1+1/n} - 2\right).$$

This is plotted as a function of ρ for $t = 0$ in Figure 5. The rate passes through zero at $\rho[2(2n+1)/(5n+3)]^{n/(n+1)}$, which is $\rho = 0.843$ for $n = 1.8$.

The physical significance of this result is that *if* one added to the model (which we do not) a distribution of accumulation (and ablation) equal to $-(\partial h/\partial t)_r$, the result would be a steady state; the upper surface would not change. The equilibrium line would be at the value of ρ just calculated. (It may be noted that the *instantaneous* effect of any accumulation and ablation that might be present could readily be accommodated within this model, because the effect would simply be to add to and subtract from the calculated thickness changes at the corresponding rates.)

At this point it is also instructive to consider the Vialov (1958) profile (Paterson, 1994), which is derived for a steady state. It was originally calculated for the case of two-dimensional (unidirectional) flow, but a Vialov-type model with a circular base of fixed radius gives the same profile, when expressed in terms of ρ and η, as the two-dimensional model, namely,

$$\rho^{1+1/n} + \eta^{2+2/n} = 1 ,$$

which is to be compared with the very similar Halfar profile (Equation (17)). The Vialov model has a uniform accumulation rate a_0 over the whole cap, which must be balanced with infinite ablation rate at the edge, the rate being

$$a = a_0 - \frac{1}{2}a_0 r_0 \delta(r - r_0) .$$

The model is internally quite consistent (provided one adds the δ-function ablation), but without accumulation and ablation the profile would instantaneously fall with uniform velocity, and the outward velocity would be infinite at the edge. Of course, this would be inconsistent with a base of fixed radius. Thus, taking the accumulation and ablation as zero in the Vialov model does not lead to a consistent result. This comparison demonstrates clearly how a small difference in the profile leads to a totally different distribution of $(\partial h/\partial t)_r$.

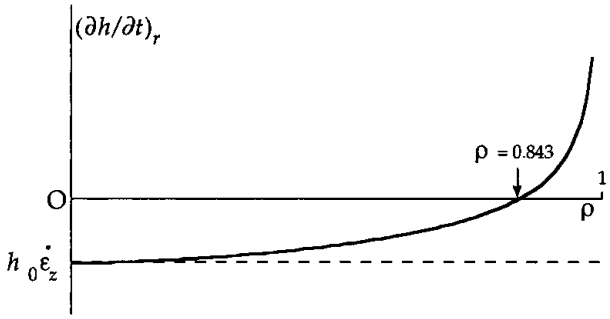

Fig. 5. The rate of increase of the thickness as a function of the fractional radial distance ρ.

5. NUMERICAL RESULTS FOR THE MARS CAPS

The central elevation is 2950 m for both caps (Zuber and others, 1998; Schenk and Moore, in press); for the north cap $T_s = 175$ K; for the south cap, $T_s = 155$ K. For the radius of the north cap, whose outline is rather irregular and uncertain, we adopt the ice volume reported by Zuber and others (1998) (1.5×10^6 km^3 for a mean value of the isostatic fraction f) and place it in a cap of central elevation 2950 m with the profile of Equation (17) (with $n = 1.8$, as justified below). This gives $R_0 = 430$ km. For the south cap we take $R_0 = 225$ km (Schenk and Moore, in press). For the north cap Zuber and others (1998) suggest that f lies between 0.15 and 0.29. For the south cap we assume the same range. Other values adopted are: $\rho' = 920$ kg m^{-3}, $g = 3.72$ m s^{-2}.

The Martian heat flux has not been measured. A nominal value often assumed, by analogy with the Earth, is $\phi_0 = 30$ mW m^{-2} and we express the flux used in the computation as a multiple λ of this; thus $\phi = \lambda\phi_0$. With $\lambda = 1$ and $f = 0.15$, $T_{\mathrm{eff}} = 196$ K for the north cap and 174 K for the south cap. With $\lambda = 1$ and $f = 0.29$ the corresponding temperatures are 201 and 179 K (giving an overall mean of 188 K).

The physical mechanism of the deformation changes with the applied stress. The flow law of Durham and others (1997), namely, $A_D = 1.26 \times 10^5$ MPa^{-n} s^{-1}, $n = 4$, $Q = 61\,000$ J mol^{-1}, is applicable for higher stresses, where dislocation creep mechanisms dominate, while that of Goldsby and Kohlstedt (1997), with $n = 1.8$, is appropriate at lower stresses where mechanisms such as grain-boundary sliding become favoured. The latter authors find that creep rate depends on grain-size d with an exponent $p = 1.4$ ($\dot{\varepsilon} \propto d^{-p}$); extrapolating their results to a grain-size of 1.0 mm (see below) gives $A_D = 62$ MPa^{-n} s^{-1}, $Q = 49\,000$ J mol^{-1}. We shall assume that both laws operate for all stresses, and that the total deformation rate is the sum of the rates from the two different processes. However, at low stresses the Goldsby and Kohlstedt mechanism will be more effective and the law will appear to have $n = 1.8$. Thus, looking first at the curve in Figure 6 for $d = 1$ mm, we see the result of taking the total shear strain rate as the sum of the

https://doi.org/10.3189/172756500781833151 Published online by Cambridge University Press

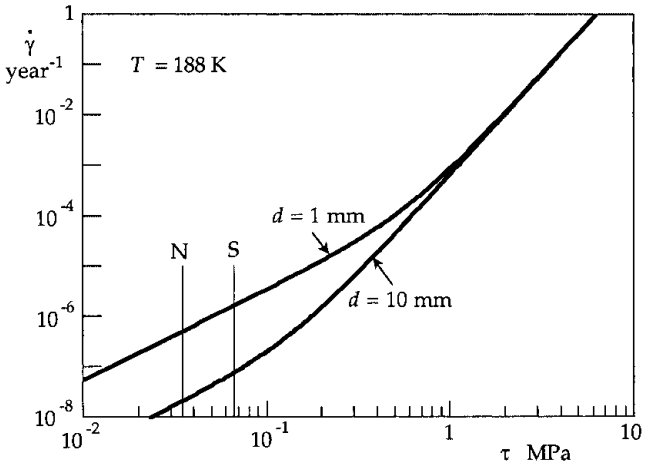

Fig. 6. The result of combining two flow laws for $n = 1.8$ and $n = 4$. The basal shear stresses estimated for the two caps are indicated.

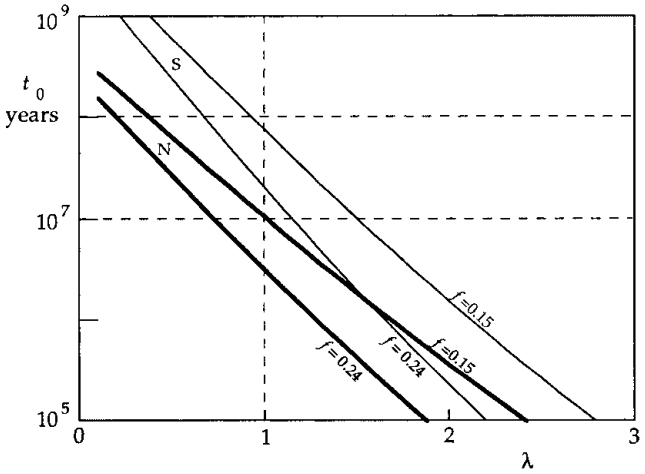

Fig. 7. The age t_0 of the caps as a function of the thermal flux, expressed as a multiple λ of 30 mW m^{-2}. Full lines: north cap; thin lines: south cap.

rates given by the two laws with $n = 1.8$ and 4, respectively. Explicitly, if subscript "i" refers to the two laws,

$$\dot{\gamma} = \sum_{i=1,2} 3^{\frac{1}{2}(n_i+1)} A_{\mathrm{D},i} \exp(-Q_i/R_\mathrm{G}T)\tau^{n_i} .$$

(The factor $3^{\frac{1}{2}(n_i+1)}$ is 4.7 for $n = 1.8$ and 15.6 for $n = 4$.)

The change in slope from 1.8 to 4 in this log-log plot occurs at the shear stress where the two rates are equal. For $T = 199$ K (north cap) the crossover is at 0.49 MPa, while for $T = 177$ K (south cap) it is at 0.74 MPa. These values must be compared with the actual stresses in the caps. The shear stress near the base of the cap at a radius where the thickness is $\frac{1}{2}H_0$ may be estimated as

$$\tau = \rho' g\,.\,h\alpha \approx \rho' g\,.\,\frac{1}{2}H_0\frac{H_0}{R_0}$$
$$= 0.035\,\mathrm{MPa}\ \text{(north cap) and}\ 0.066\,\mathrm{MPa}\ \text{(south cap)}\,.$$

Both values are well below the crossover stresses, and are therefore in the region where the flow law with $n = 1.8$ should apply. The curve in Figure 6 for $d = 10$ mm shows that this conclusion still holds for a larger grain-size. We also note that Durham and others (1992) found that up to 10% of added quartz sand has little effect on the flow properties of ice. We shall therefore use the $n = 1.8$ law, but recognizing that there are still uncertainties, which we shall refer to later; these arise primarily from the unknown preferred orientation of the crystals in relation to the stress configuration. The flow law recommended by Paterson (1994) with $n = 3$ is intermediate between the above two laws.

Figure 7 shows a semi-log plot of t_0 against λ using Equation (19). A high value of λ means greater heat flux, higher temperature at depth, weaker ice, and so a shorter lifetime t_0. Lines are shown for the two extreme values of f. The lines for the two caps are not very different, and the effect of changing f is not great.

In quoting observational evidence for the age of the caps one must distinguish them from the so-called layered deposits which appear to underlie them. The layered deposits are more extensive than the caps, especially in the south, and consist of horizontal layers of varying relative abundance of dust and water ice, which are thought to reflect climatic variations. The polar caps, on the other hand, are recognizable from their dome-shaped topography and high albedo. Although there are extensive observations, reviewed by Clifford and others (2000), the precise relation between these two geologic units remains far from clear. Crater densities on the layered deposits indicate their ages. Clifford and others (2000) quote observational evidence for an age of the exposed surface of the deposits in the north of less than about 10^5 years, and in the south of 7–15 $\times 10^6$ years. But for the caps themselves we must distinguish between the age of their surfaces and how long the bulk of their material has been there. They are very sparsely cratered and we shall tentatively assume they are 10^6 to 10^8 years old.

It is striking that, if we select the mean value $t_0 = 10^7$ years in Figure 7, the λ values for both caps fall into a fairly narrow band about $\lambda = 1.1$, although it would not have been surprising if λ had been somewhat different from this. With $t_0 = 10^8$ years the values centre on $\lambda = 0.6$.

It is as well to end on a note of caution. Strain rates in glaciology have always been notoriously difficult to calculate ab initio, because of uncertainties in extrapolating laboratory measurements to low strain rates, and in the effect of factors like grain shape, grain-size, preferred crystallographic orientation, recrystallization and bubbles. In the present problem, where grain-boundary effects are dominant, grain-size is perhaps the most troublesome unknown. Observations of the surface of the north cap (Kieffer, 1990) suggest a grain-size of 0.1 mm or more, and we have assumed 1 mm as a reasonable value at depth. A larger grain-size would lead to a smaller strain rate ($\dot{\varepsilon} \propto d^{-1.4}$), and the value of t_0 would be correspondingly increased; for example, $d = 10$ mm instead of 1 mm would raise all the curves in Figure 7 by a factor $10^{1.4} = 25.1$. The λ values for $t_0 = 10^7$ and 10^8 years would then fall in bands about $\lambda = 2.0$ and 1.4 (instead of 1.1 and 0.6).

In Figure 7 the north cap is rather younger than the south cap. The reason is revealed by using Equations (19) and (12) to find the ratio of their ages, taking n, f and H_0 to be the same for both caps:

$$\frac{t_{0,\mathrm{N}}}{t_{0,\mathrm{S}}} = \left(\frac{R_{0,\mathrm{N}}}{R_{0,\mathrm{S}}}\right)^{n+1}\frac{C_\mathrm{S}}{C_\mathrm{N}}$$
$$= \left(\frac{R_{0,\mathrm{N}}}{R_{0,\mathrm{S}}}\right)^{n+1}\exp\left[-\frac{Q}{R_\mathrm{G}}\left(\frac{1}{T_\mathrm{S}}-\frac{1}{T_\mathrm{N}}\right)\right],$$

where the subscripts "N" and "S" refer to the two caps, and T_N and T_S are the effective temperatures for $\lambda = 1$ and a mean value of f. The first factor on the right is 6.13: larger R_0 (north cap) means lower slopes and therefore smaller stresses and strain rates and longer times. The second factor

https://doi.org/10.3189/172756500781833151 Published online by Cambridge University Press

on the right is 1/40.5: higher temperature (north cap) means higher strain rates and shorter times. The temperature effect is the greater of the two opposing influences, so the calculated lifetime of the north cap is shorter by a factor 40.5/6.13 = 6.6. Clifford and others (2000) quote observations implying that the layered terrains in the north are two orders of magnitude younger that those in the south. If this difference for the layered terrains also applies to the polar ice caps, the flow model has predicted an age ratio with the same sign as that observed, but rather smaller in magnitude.

Looked at differently, Figure 7 places a constraint on the heat flux; it cannot be greater than $\lambda \approx 2.5$, because that would imply that the ice caps were younger than about 10^5 years old. As regards the possibility of basal melting (Clifford, 1987), the present model finds that this would be achieved with the present thicknesses at the centres if the heat-flux factor were $\lambda = 2.1$–2.5 (north cap) and 2.7–3.2 (south cap).

In summary, Figure 7 shows that the dimensions and surface temperature of both caps are consistent with a heat flux not far removed from that of the Earth ($\lambda = 1$), which is what is usually assumed for Mars. This supports the hypothesis that the material of both caps is flowing water ice, with an unknown amount of rock debris added.

ACKNOWLEDGEMENTS

I should like to thank W. B. Durham and R. Hindmarsh for much helpful advice, and R. LeB. Hooke and W. F. Budd for useful comments.

REFERENCES

Budd, W. F., D. Jenssen, J. H. I. Leach, I. N. Smith and U. Radok. 1986. The north polar ice cap of Mars as a steady-state system. *Polarforschung*, **56**(1–2), 43–63.

Clifford, S. M. 1987. Polar basal melting on Mars. *J. Geophys. Res.*, **92**(B9), 9135–9152.

Clifford, S. M. *and 52 others*. 2000. The state and future of Mars polar science and exploration. *Icarus*, **144**(2), 210-242.

Durham, W. B., S. H. Kirby and L. A. Stern. 1992. Effects of dispersed particulates on the rheology of water ice at planetary conditions. *J. Geophys. Res.*, **97**(E12), 20,883–20,897.

Durham, W. B., S. H. Kirby and L. A. Stern. 1997. Creep of water ices at planetary conditions: a compilation. *J. Geophys. Res.*, **102**(E7), 16,283–16,302.

Goldsby, D. L. and D. L. Kohlstedt. 1997. Grain boundary sliding in fine-grained ice I. *Scripta Materialia*, **37**(9), 1399–1406.

Haberle, R. M. and B. M. Jakosky. 1990. Sublimation and transport of water from the north residual polar cap on Mars. *J. Geophys. Res.*, **95**(B2), 1423–1437.

Halfar, P. 1981. On the dynamics of the ice sheets. *J. Geophys. Res.*, **86**(C11), 11,065–11,072.

Halfar, P. 1983. On the dynamics of the ice sheets 2. *J. Geophys. Res.*, **88**(C10), 6043–6051.

Herkenhoff, K. E. and B. C. Murray. 1990. Color and albedo of the south polar layered deposits on Mars. *J. Geophys. Res.*, **95**(B2), 1343–1358.

Hindmarsh, R. C. A. 1990. Time-scales and degrees of freedom operating in the evolution of continental ice-sheets. *Trans. R. Soc. Edinburgh, Ser. Earth Sci.*, **81**(4), 371–384.

Hobbs, P. V. 1974. *Ice physics*. Oxford, Clarendon Press.

Kieffer, H. H. 1990. H_2O grain size and the amount of dust in Mars' residual north polar cap. *J. Geophys. Res.*, **95**(B2), 1481–1493.

Melosh, H. J. 1989. *Impact cratering: a geologic process*. Oxford, Clarendon Press.

Nye, J. F. 1952. The mechanics of glacier flow. *J. Glaciol.*, **2**(12), 82–93.

Nye, J. F. 1959. The motion of ice sheets and glaciers. *J. Glaciol.*, **3**(26), 493–507.

Nye, J. F., W. B. Durham, P. M. Schenk and J. M. Moore. 2000. The instability of a south polar cap on Mars composed of carbon dioxide. *Icarus*, **144**(2), 449–455.

Paige, D. A., K. E. Herkenhoff and B. C. Murray. 1990. Mariner 9 observations of the south polar cap of Mars: evidence for residual CO_2 frost. *J. Geophys. Res.*, **95**(B2), 1319–1335.

Paterson, W. S. B. 1994. *The physics of glaciers. Third edition*. Oxford, etc., Elsevier.

Schenk, P. and J. Moore. In press. Stereo topography of the south polar region of Mars: volatile inventory and Mars Polar Lander landing site. *J. Geophys. Res.*

Smith, D. E. *and 18 others*. 1999. The global topography of Mars and implications for surface evolution. *Science*, **284**(5419), 1495–1503.

Vialov, S. S. 1958. Regularities of glacial shields movement and the theory of plastic viscous flow. *International Association of Scientific Hydrology Publication* 47 (Symposium at Chamonix 1958 — *Physics of the Movement of the Ice*), 266–275.

Zuber, M. T. *and 20 others*. 1998. Observations of the north polar region of Mars from the Mars orbiter laser altimeter. *Science*, **282**(5396), 2053–2060.

MS received 19 January 2000 and accepted in revised form 17 April 2000